Int J Artif Organs 2011; 34 (1): 54-63 DOI: 10.5301/IJAO.2011.6316

**ORIGINAL ARTICLE**

# Fibronectin distribution on demixed nanoscale topographies

*Manuel Pérez-Garnes[1*], Cristina González-García[1*], David Moratal[1], Patricia Rico[1,2], Manuel Salmerón-Sánchez[1,2,3]*

[1] Center for Biomaterials and Tissue Engineering, Universidad Politécnica de Valencia, Valencia - Spain
[2] CIBER-BBN, Bioengineering, Biomaterials and Nanomedicine, Valencia - Spain
[3] Regenerative Medicine Unit, Prince Felipe Research Center, Valencia - Spain

**The first two Authors contributed equally to this work*

ABSTRACT

Purpose: *It is known that surface nanotopography influences cell adhesion and differentiation. Our aim is to analyze the effect of nanoscale topography on fibronectin adsorption and, afterwards, on cell adhesion in order to rationalize the cell-material interaction by focusing on the state of the intermediate layer of adsorbed fibronectin at the material interphase.*

Methods: *Nanotopographic surfaces were produced by demixing of thin film polymer blends - PLLA and PS - during a high speed spin-casting process. Fibronectin (FN) was adsorbed on the different nanotopographies and the protein distribution was directly observed by atomic force microscopy (AFM). The fraction of the surface covered by the protein was quantified by image analysis, as well as the distribution of FN between peaks and valleys. Focal adhesion protein –vinculin- was immunostained and quantified by image analysis on the different nanoscale surfaces.*

Results: *Different nanoscale domains were obtained by changing the composition of the system within a height range of 3 nm to 30 nm. FN tends to adsorb on the peaks of nanoisland topographies, especially in compositions that did not enhance cell adhesion. Moreover, protein distribution between valleys and peaks alters the size of focal adhesion plaques, which grew larger on surfaces with an even distribution of fibronectin.*

Conclusions: *Our results suggest that the surface nanotopography is a key material property capable of influencing protein adsorption. Additionally, the distribution of the protein on the different samples was correlated to the initial ability of cells to adhere in terms of the size of the focal plaques.*

KEY WORDS: *Nanotopography, Protein adsorption, Fibronectin, Focal adhesion*

*Accepted: December 27, 2010*

## INTRODUCTION

Cells interact with synthetic materials via extracellular matrix (ECM) proteins, such as fibronectin (FN), vitronectin (VN), fibrinogen (FNG), previously adsorbed on the substrate surface. ECM proteins are recognized by the integrin family of cell surface receptors which provide trans-membrane links between the ECM and the actin cytoskeleton (1). Upon binding, integrins cluster and develop focal adhesions, supramolecular protein complexes that anchorage the cells to the substrate and trigger signalling events (2). Thus, the initial cell-material interaction is a complex multi-step process consisting of early events, such as adsorption of proteins, followed by cell adhesion and spreading, and late events, related to cell growth, differentiation, ECM deposition and cell functioning.

Three different kinds of physicochemical stimuli are considered to influence cell adhesion: chemistry, micro/nanotopography and stiffness (3, 4). Surface topography is a key parameter that is able to modify cell response independently of the chemical composition of the substrate, especially in terms of cell adhesion, but differentiation and gene expression can also be altered (5-7). Microfabrication techniques have been used to induce cell reorientation following microgrooves, referred to as the contact guidance phenomenon (8-10). Different nanoscale topographies have been prepared at different scales (9-100 nm) by using photolithography, electron beam lithography, colloidal lithography, and polymer demixing techniques during a high speed spin-casting process (9-12). However, the effect of nanotopography on cell response is not completely understood. It has been reported that the range from 10 nm to 30 nm improves adhesion and enhances stimulation of intracellular signaling compared to 100 nm scale (13, 14).

Since the cell-material interaction is mediated by the intermediate layer of proteins adsorbed on the surface of the material, the effect of nanotopography on cell behavior should be sought as a consequence of different protein adsorption patterns. This has already been done for other surface parameters such as wettability or chemistry but scarce experimental data exist on the effect of surface nanotopography on protein adsorption and cell response (15-19). It has been suggested that nanotopography is able to enhance protein adsorption as compared to the same plane chemistry, although no correlation has also been reported (20-22). Only a few works have focused on the effect of substrate properties on cell behavior by first addressing protein adsorption and conformation on the material surface.

Nanoscale topographies can be prepared by demixing PLLA and PS during a high speed spin-casting process (23). Either nanopits or nanoislands were obtained depending on the fraction of PLLA in the system. Initial cell adhesion was previously studied regarding the different nanofeatures (23). This work investigates the effect of surface nanotopography on protein adsorption. FN was adsorbed on the different surfaces and the distribution on the protein molecules among valleys and peaks of the surface was followed by AFM. Quantitative results were obtained by image analysis of the AFM figures. Results were correlated to cell response on the different nanomotifs in terms of focal adhesion size distributions.

## MATERIALS AND METHODS

### *Preparation of nanotopographies*

PLLA/PS thin films with different nanotopographies were obtained by spin-casting polymer solutions of different concentrations as described elsewhere (23). Briefly, PLLA (Cargill Dow, Minnetonka, MN, USA) and PS (Sigma-Aldrich, St Louis, MO, USA) were dissolved in chloroform (1 wt-%) at different ratios, 0/100, 10/30, 30/70, 50/50, 70/30, and 100/0 w/w. Spin-casting was performed on glass coverslips at 2000 rpm during 30 seconds. Samples were dried *in vacuo* at room temperature before further characterization.

### *Contact angle*

Surface wettability was characterized by measuring the water contact angle with a DataPhysics OCA 20 device (San Jose, CA, USA). Measurements were performed per quintuplicate on each substrate after adsorbing fibronectin from solutions of different concentration (0, 2, 5 and 20 µg/mL).

### *Atomic Force Microscopy*

AFM experiments were performed using a Multimode AFM equipped with NanoScope IIIa controller from Veeco (Manchester, UK) operating in tapping mode in air; the Nanoscope 5.30r2 software version was used. Si-cantilevers from Veeco (Manchester, UK) were used with force constant of 2.8 N/m and resonance frequency of 75 kHz. The phase signal was set to zero at a frequency 5% to 10% lower than the resonance one. Drive amplitude was 600 mV and the amplitude set point $A_{sp}$ was 1.8 V. The ratio between the amplitude set point and the free amplitude $A_{sp}/A_0$ was kept equal to 0.8.

Fibronectin from human plasma (Sigma, Barcelona, Spain) was adsorbed on the different substrates by immersing the material sheets in several FN solutions at concentrations of 2 µg/mL, 5 µg/mL, and 20 µg/mL in physiological solution (NaCl 0.9%) for 10 minutes. After protein adsorption, samples were rinsed in the physiological solution to eliminate the non-adsorbed protein. AFM was performed in the tapping mode immediately after sample preparation. Height, phase and amplitude magnitudes were recorded simultaneously for each image.

## Cell culture

MC3T3-E1 cells were obtained from the RIKEN CELL BANK (Ibaraki, Japan). Prior to seeding on FN-coated substrates, cells were maintained in DMEM medium supplemented with 10% fetal bovine serum and 1% penicillin-streptomycin and passaged twice a week using standard techniques.

Sample disks (12 mm diameter) placed in a 24-well tissue culture plate were coated with FN 20 µg/mL (12 h at 37°C). Then, $10^3$ cells were placed onto each substrate and were maintained at 37°C in a humidified atmosphere under 5% $CO_2$ for 3 hours. Each experiment was performed in triplicate.

## Cell adhesion

After 3 hours of culture, MC3T3-E1 cells were washed in Dulbecco's phosphate-buffered saline (DPBS; Invitrogen, Carlsbad, CA, USA) and fixed in 10% formalin solution (Sigma, Barcelona, Spain) at 4°C for 1 hour. Samples were then rinsed with DPBS and a permeabilization buffer (103 g/L sucrose, 2.92 g/L NaCl, 0.6 g/L $MgCl_2$, 4.76 g/L HEPES buffer, 5 ml/L Triton X-100, pH 7.2) was added at room temperature for 5 minutes. In order to reduce the background signal, samples were incubated in 1% BSA/DPBS at 37°C for 5 minutes. Afterwards, samples were incubated in monoclonal mouse antibody against vinculin (1:400 in 1% BSA/DPBS; Sigma, Barcelona, Spain) at room temperature for 1 hour. The samples were rinsed in 0.5% Tween-20/DPBS three times for 5 minutes each. Alexa fluor 633-conjugated rabbit anti-mouse secondary antibody (1:200 in 1% BSA/DPBS; Invitrogen, Carlsbad, CA, USA) was then added at room temperature for 1 hour. Simultaneously, BODIPY FL phallacidin was added for the duration of this incubation (2 to 3 units/sample in 1% BSA/DPBS; Invitrogen, Carlsbad, CA, USA). Finally, samples were washed before being mounted in Vectashield containing DAPI (Vector Laboratories, Peterborough, UK). A Leica DM6000B fluorescent microscope was used for cellular imaging.

## Image analysis

All image processing and analysis was done using in-house software developed under MATLAB R2009b (The MathWorks, Inc., Natick, MA, USA).

For calculating the distribution of FN between valleys and pits, the valleys and the pits were first delineated. To do this, the height AFM image was grey scaled and equalized, providing an output grayscale image with its intensity values evenly distributed throughout the intensity range, and then a median filtering was applied to the resulting image to reduce noise background. This new image was then binarized through Otsu's method (24), which chooses the threshold that minimizes the intraclass variance of the thresholded black and white pixels, providing a binary image with the valleys and the pits perfectly segmented. The contour of the pits was then easily extracted and applied, in a second step, to the amplitude and phase AFM images.

FN was detected from the amplitude AFM images. It was subsequently associated to the valleys or to the pits based on the contour between them, both previously detected using the height AFM images, and the results were averaged. For this procedure, several steps were followed: (i) both images were firstly gray- scaled, equalized and a median filtering was applied to the resulting images for background noise reduction. The histogram of both images was then automatically stretched for a fair detection of the protein. The images were then size-filtered to avoid the detection of regions that were too small, thus not corresponding to proteins. Once the protein was correctly detected, it was associated with a valley or a pit based on the contour previously detected from the height AFM image.

The size distribution of the focal plaques was determined through a multi-step image analysis, including a contour delineation of the cell. To achieve perfect segmentation of the cell, firstly, images showing the actin cytoskeleton were gray-scaled and equalized. Secondly, the cell was then detected (segmented): since the cytoskeleton differed greatly in contrast from the background image, a gradient-magnitude method (Sobel) was applied to the image and once the gradient image was calculated, a binary mask was created containing the segmented cytoskeleton (25-27). Thirdly, when compared to the original image, the binary gradient mask showed gaps in the lines surrounding the cell (the outline of the object of interest was not completely delineated). These linear gaps disappeared when the Sobel image was dilated using linear structuring elements (a vertical structuring element followed by a horizontal one), obtaining a clear and perfect contour detection of the cell. Once the cell was perfectly segmented, the obtained binary mask was then applied to the image obtained in the red channel for vinculin. This made it possible to focus

attention on the cell and the focal adhesions since any other object in the image was virtually erased. This new image was then binarized through Otsu's method and size-filtered to avoid any extra small particles in the image that did not represent focal plaques with sizes that fit the study aims (24). Once the sizes of the focal contacts were determined, a size distribution was easily obtained.

### *Statistics*

All experiments were performed at least three times in triplicate unless otherwise noted. Data are reported as mean-standard error. Results were analyzed by one-way ANOVA using SYSTAT 8.0 (SPSS, Chicago, IL, USA). If treatment level differences were determined to be significant, pairwise comparisons were performed using a Tukey post hoc test. A 95% confidence level was considered significant.

## RESULTS AND DISCUSSION

### *Nanoscale topographies*

Figure 1 shows AFM height images of PLLA/PS nanotopographies as obtained during polymer demixing in a high speed spin-casting on glass coverslips at various ratios of the base components (PLLA/PS): 0/100, 10/90, 30/70, 50/50, 70/30, 90/10, and 100/0. Nanotopographic motifs are found for every intermediate composition, referred to as interconnected pits, for the substrates with PLLA content below 50% (included) and isolated islands above 50% PLLA. That is to say, the materials surface consists of valleys and peaks with a characteristic geometric distribution (Fig. 1). The height of the elevated areas in the sample depends non-monotonically on the PLLA content, as shown in the sections displayed in Figure 1 and the corresponding quantification in Figure 2: sub-10 nm features are found for low and high PLLA contents (10/90, 90/10) and similar 20 nm ones for the intermediate compositions. By contrast, the fraction of the surface area covered by raised nanofeatures decreases linearly as the amount of PLLA in the sample increases (Fig. 2). These results are in agreement with those values previously reported for this system (23).

Even though surface topography is often only a manifestation of the underlying chemistry, it can also be modulated in an independent way. For the system prepared in this work, it is known that PLLA tends to be segregated onto the top surface, as obtained from SIMS and XPS (20). That is to say, this system consists of nanotopographies with different geometrical patterns whose surface consists mostly of PLLA, especially for samples which have a total PLLA content higher than 30%. That is to say, the effect on cell

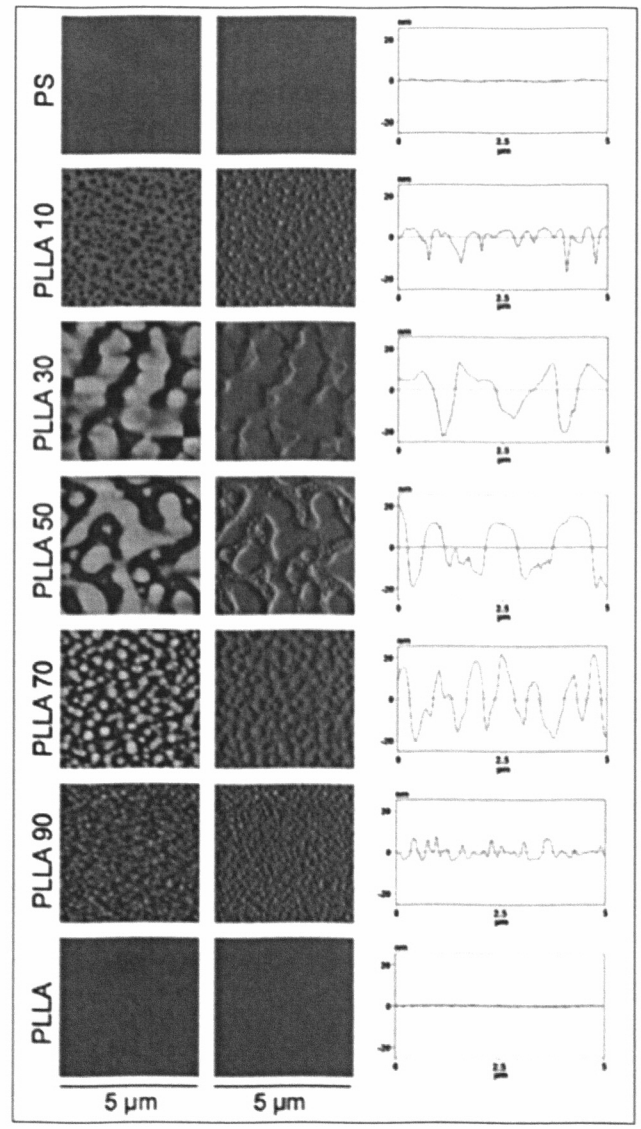


**Fig. 1** - *AFM images for the PLLA/PS demixed nanotopographies as obtained after spin-casting from solutions of different polymer ratios. First two columns show the height and amplitude magnitudes in AFM, while the third one is a transversal cut.*

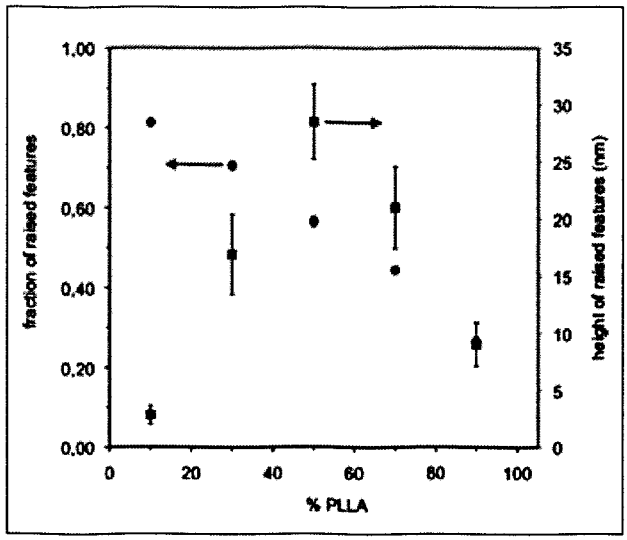


**Fig. 2** - *Fraction of raised features (circles) and their average height (squares) as calculated from AFM images for the different nanotopographies. Error bar represents the standard deviation of three independent areas on the sample. When not visible, it is smaller than the symbol.*

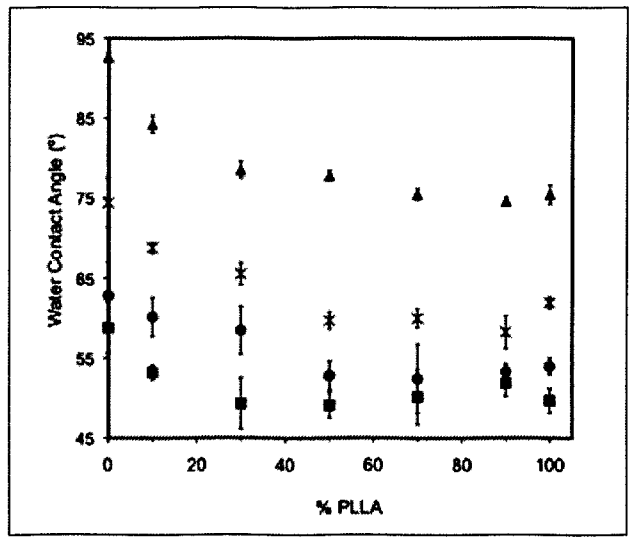


**Fig. 3** - *Water contact angle on the different nanoscale topographies as measured on the plane surface (triangles) and after adsorption of FN from solutions of different concentrations: 2 µg/mL (stars), 5 µg/mL (circles) and 20 µg/mL (squares).*

behavior must be ascribed to different nanometric patterns rather than to the effect of surface chemistry. The surface of the sample with 10% PLLA consists of approximately 70% PLLA (20). For this reason, the water contact angle decreases from 93° for the hydrophobic PS to 85° for the sample with 10% PLLA (but with 30% PS on the surface) and then it stabilizes at approximately 75° for the rest of the samples, supporting the presence of similar PLLA surface chemistries, regardless of the underlying nanotopography obtained as a consequence of the phase separation process during spin-casting (Fig. 3).

## *Fibronectin adsorption and distribution*

Figure 4 shows the AFM amplitude magnitude at several magnifications for the different nanotopogaphies after FN adsorption from 2 µg/mL solutions. FN molecules are unambiguously identified on each substrate, while the height magnitude (Fig. 1) can be used for simultaneously identifying the spatial distribution of FN throughout the peaks and valleys in the sample. Only isolated molecular aggregates are observed on each sample, homogeneously distributed throughout the surface. Likewise, the water contact angle decreased approximately 20° after FN adsorption, independently of the composition of the sample (Fig. 3). Moreover, increasing the concentration of the solution from which FN is adsorbed leads to a further increase in surface wettability (Fig. 3), but the water contact angle follows the same qualitative trend previously found on the bare substrates.

Image analysis of the AFM figures allows one to quantify the distribution of protein molecules between the pits and valleys of the nanostructure. Figure 5a shows that the fraction of the area covered by FN remains below 0.2 for both the PLLA and the 10% PLLA substrates and then it increases slightly, by up to approximately 0.25, for the rest of the samples. The distribution of the protein between high and low areas in the surface has also been included in Figure 5a. As the amount of PLLA in the sample increases, the fraction of FN on raised nanofeatures (circles in Fig. 5a) decreases. Consequently, as the total amount of adsorbed FN remains approximately constant (stars in Fig. 5a), the fraction of FN on the valleys of the surface increases as the amount of PLLA in the sample increases. At first sight, this analysis suggests that the distribution of FN between valleys and peaks is a mere consequence of the nanotopographic structure of the system, since the fraction of elevated peaks decreases as the amount of PLLA in the

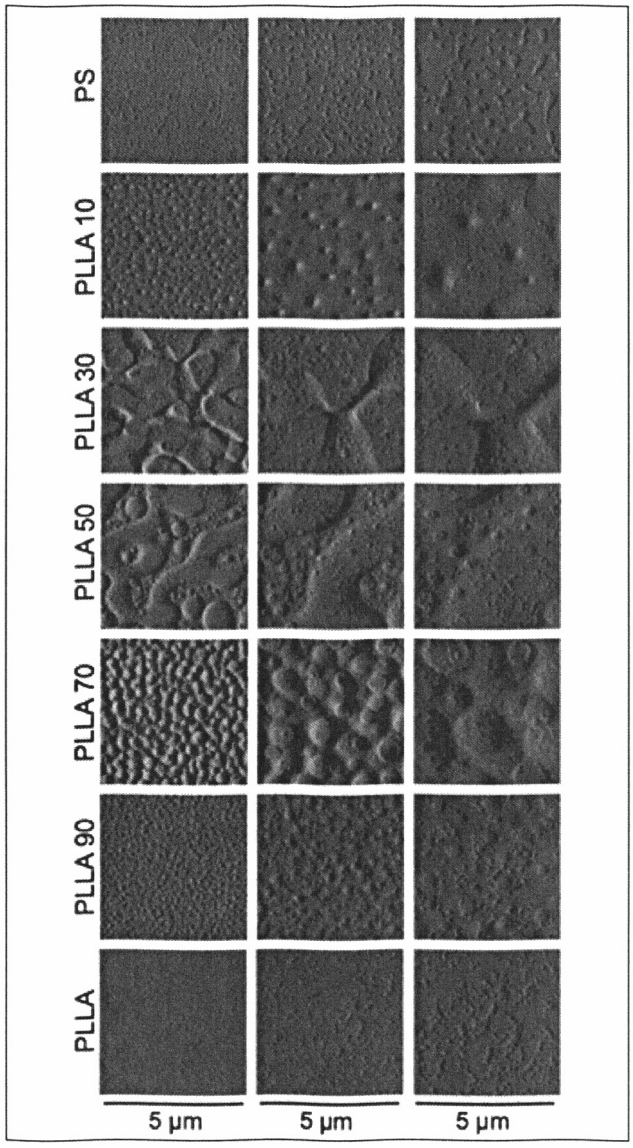


**Fig. 4** - *AFM images (amplitude) at different magnifications for the different nanoscale topographies after FN adsorption from a solution of concentration 2 µg/mL. The corresponding height magnitude (not shown) allows one to identify the peaks and valleys in the surface while the phase magnitude provides direct observation of FN distribution throughout the sample.*

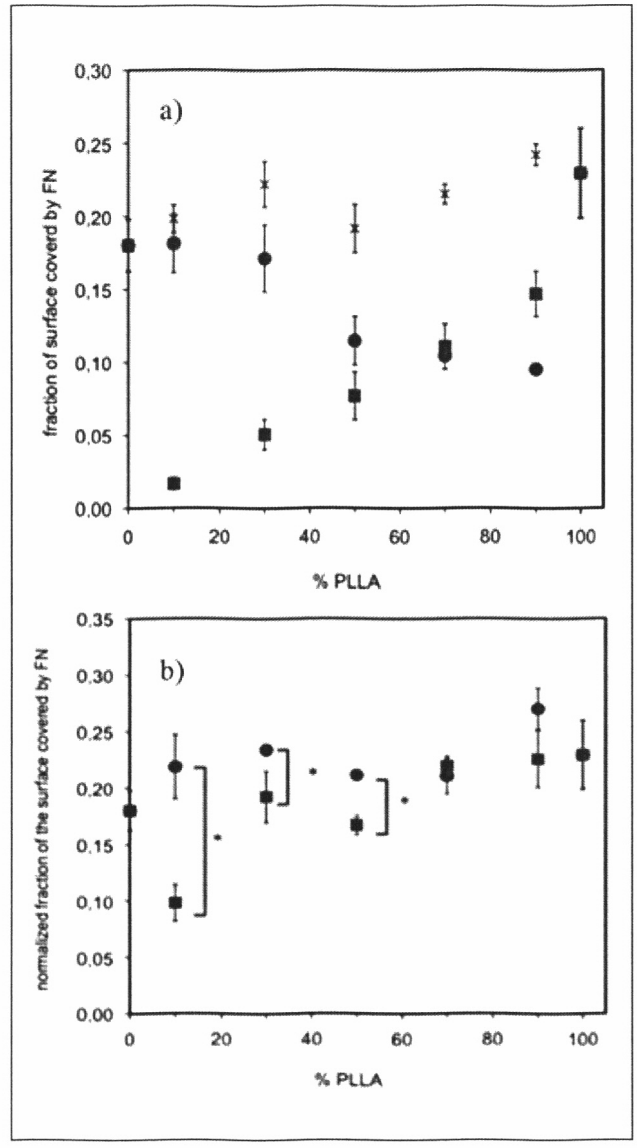


**Fig. 5** - *Fraction of the surface covered by FN as obtained from image analysis:* ***a)*** *total fraction of the area covered by FN (stars) and its distribution between peaks (circles) and valleys (squares);* ***b)*** *Fraction of the area covered by FN per unit area of peaks (circles) and valleys (squares). Star represents statistical difference with p=0.05.*

sample decreases (Fig. 2) and, also, surface chemistry is maintained regardless of the bulk composition of the substrate (Fig. 2). A more thorough analysis shows that this is not the entire story. Figure 5b shows the fraction of the surface covered by the protein by taking into account the actual area occupied by the valleys and peaks on each substrate. That is to say, circles in Figure 5b represent the area occupied by FN adsorbed on raised nanofeatures per unit area of raised nanofeatures. Likewise, squares in Figure 5b represent the same magnitude for the valleys

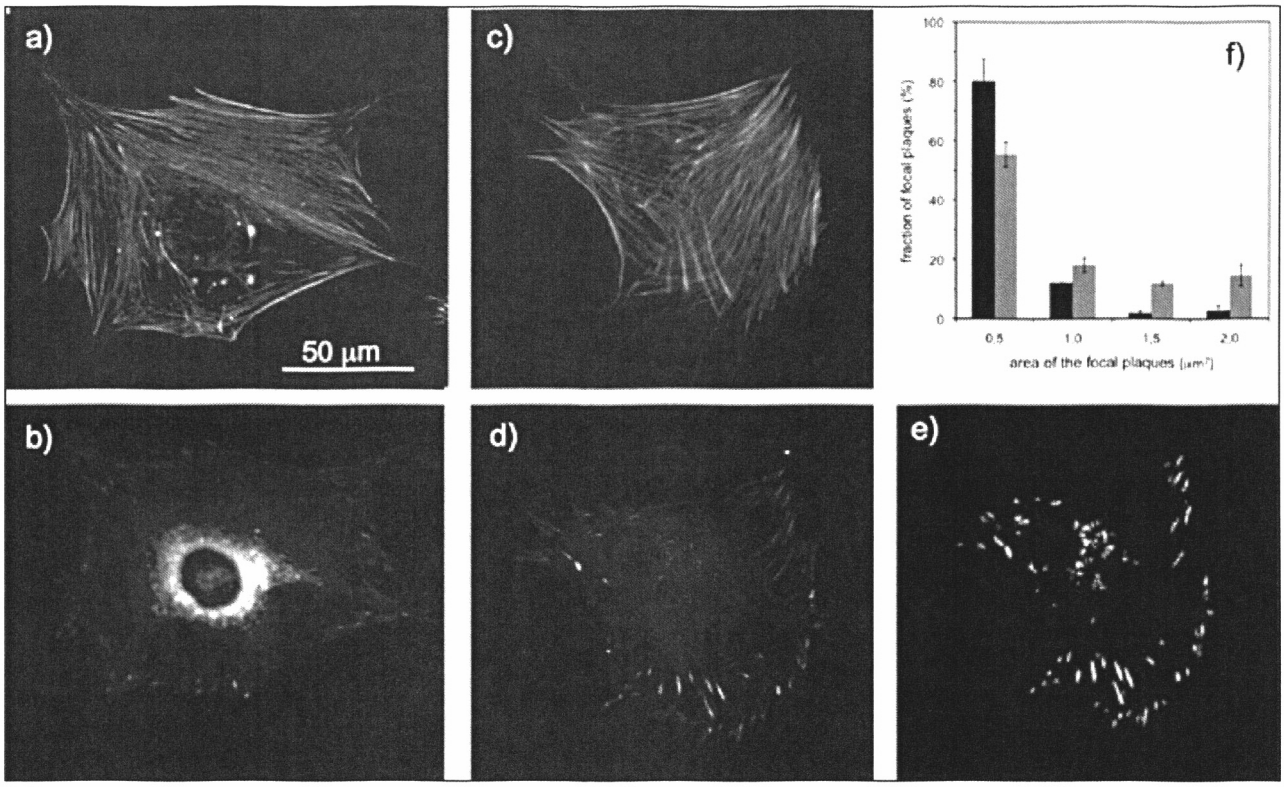


**Fig. 6 -** *MC3T3-E1 osteoblast-like cells after 3 hours of culture on different nanoscale topographies:* ***(a, c)*** *actin cytoskeleton;* ***(b, d)*** *immunofluorescence for vinculin; (a-b) represents a cell on nanofeatures obtained with PLLA lower than 50%, i.e., on which there is a difference between the amount of FN adsorbed on valleys and peaks (see Fig. 5b); (c-d) represents a cell on nanofeatures with PLLA higher than 50%, i.e., on which FN is evenly distributed between valleys and peaks (see Fig. 5b). The size distribution of focal adhesion plaques was calculated for different cells on each family of surfaces by image analysis;* ***(e)*** *represents the cell obtained from (d) after the image processing to select focal plaques. The corresponding hystogram for both kind of cells (for cells like the one in (a)-black, for cells like the one in (c)-gray) is shown in* ***(f)****. Pair-wise comparisons were performed using a Tukey post hoc test. Differences between black and gray bars were found to be significant with a 95% confidence level for every area of the focal plaques.*

of the nanostructure. Had the distribution of FN between valleys and peaks been a mere reflect of high and low areas in the sample, circles and squares should account for the same value in Figure 5b. However, it is revealed that FN tends to be adsorbed on the raised features of the nanotopography, regardless of the underlying geometrical distribution of either pits or islands. The difference is especially large for the sample with 10% PLLA, but is also statistically meaningful ($p < 0.05$) between high and low areas of the surface for the substrates with 30% and 50% PLLA (Fig. 5b). A higher amount of PLLA in the system leads to an even distribution of FN between valleys and peaks of the sample.

## *Cell behavior as a consequence of fibronectin distribution*

Though the effect of surface nanotopography on cell behavior should be a consequence of different protein adsorption patterns, scarce experimental data exist on the effect of surface nanotopography on protein adsorption. It has been suggested that micro and nanotopography are able to enhance protein adsorption as compared with the same plane chemistry (20, 21, 28). Cells cultured on these substrates displayed enhanced cell density and spreading on the substrates containing higher amounts of PLLA (70% and 90% PLLA) (23). It has been suggested that this

effect might be a consequence of the total area difference including sidewalls, or the different coarseness of texture (23). Despite the belief that the cell-protein-material interaction is of fundamental importance for understanding the role of materials in biomedicine, clear links between the material surface properties, the adsorbed protein layer and their influence on the cell remain far from understood. Even if some efforts have been devoted to the influence of material chemistry, clear correlations between nanotopography, protein adsorption and cell behavior have not been established yet (15, 16, 29-32). Our results on fibronectin adsorption, showing that approximately the same amount of protein is adsorbed on the different nanotopographies but with uneven distribution, rationalizes the cellular results previously found on these substrates in terms of the number of adhered cells and their spreading area (23). That is to say, for substrates where there is no difference in the fraction of adsorbed protein between peaks and valleys (70% and 90% PLLA) cells adhere and spread better (23) as compared to the nanofeatured surfaces on which FN is especially available on the upmost surface (10%, 30%, 50% PLLA). The fact that nanotopography is able to alter the distribution of adsorbed FN between high and low areas has been recently shown on a similar system, which also consists of PLLA/PS demixed topographies but with the same 50% composition and a different final concentration of the spinning solution (21).

Interestingly, even if the underlying topography was found to influence the total number of cells and the spreading area (23), we found F-actin cytoskeleton formation and well-developed focal adhesions on each substrate, independently of the nanofeature distribution and size. Two representative cells for each one of the substrates on which FN distribution occurs differently are shown in Figure 6, showing significant differences between the protein density in valleys and on peaks: nanofeatures with PLLA lower than 50% (Figs. 6a-b, in which FN tends to adsorb preferentially on the peaks) and the substrates with higher PLLA contents (Figs. 6c-d, with even an distribution of FN between valleys and peaks). Larger focal contacts seem to be formed on those substrates with a PLLA content higher than 50%. Image analysis allows one to calculate the distribution of focal adhesion plaques (Figs. 6 e-f). Approximately 80% of focal plaques are smaller than 1 $\mu m^2$ for cells adhered on substrates with low PLLA contents. By contrast, approximately 50% of the focal plaques are larger than 1 $\mu m^2$ for cells on substrates with a higher PLLA fraction. It has been reported that cells were able to form larger focal contacts on nanostructure materials (6, 21). Vinculin level at adhesion sites has been correlated in a linear manner with tractional forces exerted by cells, so that tension needs to be developed between the ECM and the adhesion site for vinculin recruitment (33, 34). The formation of mature focal adhesions occurs through integrin clustering via increased force generated by the cytoskeleton (35); conversely, less mature cytoskeleton suggests that less tension is applied to integrins, resulting in less clustering and smaller contacts (36). We have not found any difference in the state of development of actin cytoskeleton on the different nanotopographies (Fig. 6), which suggests that the size of the adhesion contacts, directly modulated by the available FN between valleys and peaks, is large enough to facilitate cell contractility and cytoskeleton development.

## CONCLUSIONS

Our results suggest that surface nanotopography is a key material property capable of influencing protein adsorption. Specifically, nanofeatures lead to enhanced protein distribution of FN between the peaks and valleys of the nanostructure for nanopit topography and uneven distribution between high and low areas of the sample for isolated nanoislands of approximately 20 nm height. Moreover, the distribution of the protein on the different samples was correlated to cell behavior. Enhanced cellular response was found on surfaces that provide more geometrical input to cells, that is to say, surfaces on which FN distributes evenly between valleys and peaks. The size distribution of focal plaques was modified by the underlying nanotopography as a consequence of the distribution of FN between valleys and peaks.

## ACKNOWLEDGEMENTS

*AFM was performed under the technical guidance of the Microscopy Service at the Universidad Politécnica de Valencia, whose advice is greatly appreciated.*

**Financial support:** This studied was funded by the Spanish Ministry of Science and Innovation through MAT2009-14440-C02-01 and TEC2009-14128 grants. CIBER-BBN is an initiative funded by the VI National R&D&i Plan 2008-2011, Iniciativa Ingenio 2010, Consolider Program, CIBER Actions and financed by the Instituto de Salud

Carlos III with assistance from the European Regional Development Fund. This work was supported by funds for research in the field of Regenerative Medicine through the collaboration agreement with the Conselleria de Sanidad (Generalitat Valenciana), and the Instituto de Salud Carlos III.

**Conflict of interest statement:** Authors declare no conflict of interest.

Address for correspondence:
Manuel Salmerón-Sánchez
Center for Biomaterials and Tissue Engineering
Universidad Politecnica de Valencia
Camino de Vera s/n, 46022
Valencia, Spain
e-mail: masalsan@fis.upv.es

## REFERENCES

1. Hynes RO. Integrins: bidirectional, allosteric signaling machines. Cell 2002; 110: 673-87.
2. Grinnell F. Focal adhesion sites and the removal of substratum-bound fibronectin. J Cell Biol 1986; 103: 2697-706.
3. Wong JY, Leach JB, Brown XQ. Balance of chemistry, topography and mechanics at the cell biomaterial interface: Issues and challenges for assessing the role of substrate mechanics on cell response. Surf Sci 2004; 570: 119-33.
4. Schwarz US, Bischofs IB. Physical determinants of cell organization in soft media. Med Eng Phys 2005; 27: 763-72.
5. Zinger O, Zhao G, Schwartz Z, et al. Differential regulation of osteoblasts by substrate microstructural features. Biomaterials 2005; 26: 1837-47.
6. Dalby MJ, Gadegaard N, Tare R, et al. The control of human mesenchimal cell differentiation using nanoscale symmetry and disorder. Nat Mater 2007; 6: 997-1003.
7. Dalby MJ, MCCloy D, Robertson M, Wilkinson CD, Oreffo RO. Osteoprogenitor response to defined topographies with nanoscale depths. Biomaterials 2006; 27: 1306-15.
8. Ohara PT, Buck RC. Contact guidance in vitro. A light, transmission, and scanning electron microscopic study. Exp Cell Res 1979; 121: 235-49.
9. Lim JY, Donahue HJ. Cell sensing and response to micro- and nanostructured surfaces produced by chemical and topographical patterning. Tissue Eng 2007; 13: 1879-91.
10. Affrossman S, Jerome R, O'Neill SA, Schmitt T, Stamm M. Surface structure of thin films of blends of polystyrene and poly(n-butyl methacrylate). Colloid Polym Sci 2000; 278: 993-9.
11. Denis FA, Hanarp P, Sutherland DS, Dufrene YF. Fabrication of nanostructures polymer surfaces using colloidal litography and spin coating. Nano Lett 2002; 2: 1419-25.
12. Vieu C, Carcenac F, Pepin A, et al. Electron bean litography : resolution limits and applications. Appl Surf Sci 2000; 164: 111-7.
13. Lim JY, Dreiss D, Zhou Z, et al. The regulation of integrin-mediated osteoblast focal adhesion and focal adhesion kinase expression by nanoscale topography. Biomaterials 2007; 28: 1787-97.
14. Dalby MJ, Hart A, Yarwood SJ. The effect of RACK1 signalling protein on the regulation of cell adhesion and cell contact guidance on nanometric grooves. Biomaterials 2008; 29: 282-9.
15. Keselowsky BG, Collard DM, García AJ. Surface chemistry modulates focal adhesion composition and signaling through changes in integrin binding. Biomaterials 2004; 25: 5947-54.
16. Keselowsky BG, Collard DM, García AJ. Surface chemistry modulates fibronectin conformation and directs integrin binding and specificity to control cell adhesion. J Biomed Mater Res A 2003; 66: 247-59.
17. Altankov G, Groth T. Reorganization of substratum-bound fibronectin on hydrophilic and hydrophobic materials is related to biocompatibility. J Mater Sci Mater Med 1994; 5: 732-7.
18. Altankov G, Groth T. Fibronectin matrix formation and the biocompatibility of materials. J Mater Sci Mater Med 1996; 7: 425-9.
19. Rodríguez Hernández JC, Rico P, Moratal D, Monleón Pradas M, Salmerón Sánchez M. Fibrinogen patterns and activity on substrates with tailored hydroxyl density. Macromol Biosci 2009; 9: 766-75.
20. Khor HL, Kukula H, Tamada K, Knoll W, Moeller M, Hutmacher DW. Response of cells on surface-induced nanopatterns: fibrolasts and mesenchimal progenitor cells. Biomacromolecules 2007; 8: 1530-40.
21. González-García C, Sousa SR, Moratal D, Rico P, Salmerón-Sánchez M. Effect of nanoscale topography on fibronectin adsorption, focal adhesion size and matrix organization. Col Surf B 2010; 77: 181-90.
22. Cai K, Bossert J, Jandt K. Does nanometre scale topography of titanium influence protein adsorption and cell proliferation? Col Surf B 2006; 49: 136-44.
23. Lim JY, Hansen JC, Siedlecki CA, et al. Osteoblast adhesion on poly(L-lactic acid)/polystyrene demixed thin film blends: Effect of nanotopography, surface chemistry and wettability. Biomacromolecules 2005; 6: 3319-27.
24. Otsu N. A Threshold Selection Method from Gray-Level Histograms. IEEE Trans Syst Man Cybern 1979; 9: 62-6.

25. Gonzalez RC, Woods RE, Eddins SL. Digital Image Processing using MATLAB. Upper Saddle River, NJ: Prentice-Hall; 2003.
26. Gonzalez RC, Woods RE. Digital Image Processing. Upper Saddle River, NJ: Prentice-Hall; 2007.
27. MATLAB Image Processing Toolbox User's Guide. Natick, MA: The MathWorks, Inc.; 2006.
28. Pegueroles M, Aparicio C, Bosio M, et al. Spatial organisation of osteoblast fibronectin matrix on titanium surfaces: effects of roughness, chemical heterogeneity and surface energy. Acta Biomater 2010; 6: 291-301.
29. Allen LT, Tosetto M, Miller IS, et al. Surface-Induced changes in protein adsorption and implications for cellular phenotypic responses to surface interaction. Biomaterials 2006; 27: 3096-108.
30. Gugutkov D, Altankov G, Rodríguez Hernández JC, Monleón Pradas M, Salmerón Sánchez M. Fibronectin activity on substrates with controlled-OH density. J Biomed Mater Res A 2010; 92: 322-31.
31. Lee MH, Ducheyne P, Lynch L. Boettiger, Composto RJ. Effect of biomaterial surface properties on fibronectin-alpha$_5$ beta 1 integrin interaction and cellular attachment. Biomaterials 2006; 27: 1907-16.
32. Costa Martínez E, Rodríguez Hernández JC, Machado M, et al. Human chondrocyte morphology, its dedifferentiation and fibronectin conformation on different PLLA microtopographies. Tissue Eng Part A 2008; 14: 1751-62.
33. Dalby MJ, McCloy D, Robertson M, et al. Osteoprogenitor response to semi-ordered and random nanotopographies. Biomaterials 2006; 27: 2980-7.
34. Dalby MJ. Topographically induced direct cell mechanotransduction. Med Eng Phys 2005; 27: 730-42.
35. Galbraith CG, Yamada KM, Sheetz MP. The relationship between force and focal complex development. J Cell Biol 2002; 159: 695-705.
36. Balaban NQ, Schwarz US, Riveline D, Goichberg P, Tzur G, Sabanay I. Force and focal adhesion assembly: a close relationship studied using elastic micropatterned substrates. Nat Cell Biol 2001; 3: 466-72.